Springer

Acta Mechanica Sinica

CrossMark click for updates

• RESEARCH PAPER •

Acta Mech. Sin., Vol. 39, 322290 (2023)
https://doi.org/10.1007/s10409-022-22290-x

An analytical model for maximum temperature and temperature distribution of plate structure with active cooling

Guohao Hu[1,2], Fengquan Zhong[1,2*], and Keting Chen[1,2]

[1] *State Key Laboratory of High Temperature Gas Dynamics, Institute of Mechanics, Chinese Academy of Sciences, Beijing 100190, China;*
[2] *School of Engineering Science, University of Chinese Academy of Sciences, Beijing 100049, China*

Received September 28, 2022; accepted November 21, 2022; published online January 12, 2023

Plate structures with active cooling are widely used, and rapid evaluation of the temperature performance is of interest. In this paper, an analytical model is proposed for the prediction of maximum temperature and temperature distribution of plate structures with active cooling channel. The analytical model has three types of input parameters including thermal boundary conditions, material properties, and geometry parameters. Solution procedures under different thermal boundary conditions, including heat flux and convective heat transfer, are discussed respectively. The model with heat flux boundary (MHF) is established based on the principle of energy conservation. The model with convective heat transfer boundary (MCHT) is established based on the method of second-order function fitting the real heat flux distribution. The materials of the plate structures are aluminum alloy and titanium alloy. The results show that the analytical model is able to predict the maximum temperature with an error of less than 4% compared to the numerical method. The analytical model is able to quickly and accurately evaluate the thermal protection performance of the active cooling structure.

Plate structure, Active cooling, Thermal protection, Convective heat transfer, Analytical model

Citation: G. Hu, F. Zhong, and K. Chen, An analytical model for maximum temperature and temperature distribution of plate structure with active cooling, Acta Mech. Sin. **39**, 322290 (2023), https://doi.org/10.1007/s10409-022-22290-x

Nomenclature

T	Temperature, K
q	Heat flux, W/m^2
δ	Thickness, m
d	Diameter, m
W	Width of plate/channel spacing, m
k	Thermal conductivity of coolant, W/(m K)
λ	Thermal conductivity of solid, W/(m K)
h	Convective heat transfer coefficient of hot gas, W/(m^2 K)

Abbreviation

MHF	Model with heat flux boundary
MCHT	Model with convective heat transfer boundary
RMSE	Root mean squared error

Subscripts

channel	Channel wall
f	Fluid
max	Maximum
hot	Hot gas
wall	Surface
A, B, C	Position

1. Introduction

Active cooling has been widely used for the thermal protection of hypersonic vehicles [1-5], photovoltaic [6-9], and lithium-ion battery [10-13] applications due to its flexible design and reliable structure. Taddeo et al. [14,15] experimentally studied the performance of active cooling of hydrocarbon fuel for scramjet applications. The effect of mass

*Corresponding author. E-mail address: fzhong@imech.ac.cn (Fengquan Zhong)
Executive Editor: Jianqiang Chen

flow rate on the heat transfer efficiency of the cooling system was experimentally investigated using ethylene as coolant. Ebaid et al. [16] used Al_2O_3 and TiO_2 nanofluids to cool photovoltaic panels and the experimental results showed that cooling of nanofluids may greatly reduce the surface temperature of photovoltaic panels and improve photoelectric efficiency. Akbarzadeh et al. [17] proposed a "hybrid cooling plate" method that combines water cooling and phase change material of paraffin/graphite to cool down lithium-ion batteries. Experimental and numerical results show that the "hybrid cooling plate" method can reduce the energy consumption caused by active cooling while meeting the cooling requirements.

There are a large number of plate structures of engineering objects that require thermal protection [18-21], such as rocket or scramjet engines [22], reusable aircraft bodies [23-25], and electronic components. There are wide areas of plate structures on hypersonic aircraft that require active cooling due to the intense heat generated by fuel combustion and aerodynamic heating. Youn et al. [26] optimized the channel parameters of the cooling plate on the hypersonic aircraft. The results showed that the size of the cooling channel is recommended to be smaller because the pressure drop caused by it can be ignored. Wagner et al. [27] summarized the regenerative cooling technology used to cool rocket thrust chambers and orbital vehicles. The characteristics of hydrogen, oxygen, and hydrocarbon fuels as coolants are studied, and the repeatable service life of the thrust chamber is also analyzed. The research results show that regenerative cooling is a key technology for aircraft to realize reusability. Li et al. [28] designed a plate-type microchannel-heat-exchanger used for active cooling the electronic components on spacecraft.

The actively thermal protection system is a complex system coupled with fluids and solids. Experimental and numerical methods are typically used to evaluate the cooling effect. However, both methods are complex and time consuming. In this paper, an analytical model is proposed to quickly predict the maximum temperature and temperature distribution of plate structure with active cooling channel. The coolant is chosen to be kerosene. The material of the plate is chosen to be aluminum alloy or titanium alloy. It is worth mentioning that the analytical model is also usable for other coolants and plate materials. Two solution procedures of the analytical model are established based on different thermal boundary conditions. The model accuracy is validated by the numerical results.

2. Analytical model setup and boundary conditions

The schematic diagram of the plate structure with active cooling channel is shown in Fig. 1a. A cooling structure with circular cooling channel is located beneath the plate. The thermal boundary of the plate top surface is heat flux (the second thermal boundary) or convective heat transfer (the third thermal boundary). The other surfaces are adiabatic except for the cooling channel wall with convective heat transfer.

The schematic diagram of a cross section of the plate structure is shown in Fig. 1b. Heat transfer in the three-dimensional (3D) plate structure may be simplified to two-dimensional (2D) heat transfer through the cross sections of the plate structure because heat conduction along with the plate streamwise (z) direction is much smaller than that in the vertical and spanwise (y, x) directions. The streamwise change in coolant properties is neglected for cases with a small temperature rise of coolant through the cooling channel, which applies to the structure with relatively low heat flux and short length. The 2D heat transfer of cross sections is then divided into two segments, 0-1 segment and 1-2 segment. The length of the 0-1 segment is X, and the maximum temperature is located at the 0 point as indexed as T_0. The height and width of the 1-2 segment are $\Delta H = \delta + H_2/2$ and H_1, respectively. T_{channel} is the average inner wall temperature of the cooling channel, which can be determined

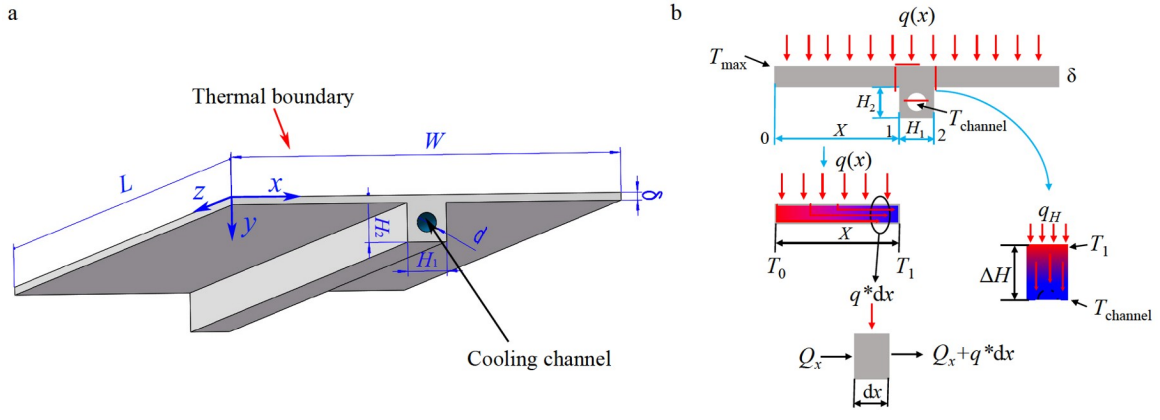

Figure 1 Schematic diagram of the plate with active cooling **a** 3D configuration and **b** simplified 2D configuration.

using the empirical formula of convective heat transfer as addressed in the later section.

2.1 Analytical model

As shown in Fig. 1a, the plate thickness is δ and the length of section 0-1 is $X = (W-H_1)/2$, where W is the channel spacing i.e., the width of the plate as shown in Fig. 1a. The size of the rectangular cooling structure beneath the plate is $H_1 \times H_2$. $q(x)$ is the heat flux on the plate top surface.

2.1.1 0-1 segment

The heat flux in the 0-1 segment is mainly conducted along the x-direction due to the large value of the length-to-height ratio. q_x is heat flux in the x-direction at the x position. Thermal analysis of an elemental section in the 0-1 segment is shown in Fig. 1b. According to the differential formula [29] for heat conduction through an elemental section, the heat flux in the spanwise direction at x position for the thermally steady state, q_x, is obtained by integration as shown below.

$$q_x = \frac{Q_x}{\delta} = \int_0^x \frac{q(x)\mathrm{d}x}{\delta}, \tag{1}$$

where Q_x denotes the total heat in the section from 0 to x position.

According to Fourier's law [30]:

$$\mathrm{d}T = -\frac{q_x \mathrm{d}x}{\lambda}, \tag{2}$$

where λ is the thermal conductivity of the plate material.

Integrate both sides of formula (2):

$$\int_0^x \mathrm{d}T = \int_0^x -\frac{q_x \mathrm{d}x}{\lambda} = T_x - T_0. \tag{3}$$

Therefore, the maximum temperature $T_{\max}$ is

$$\begin{cases} T_{\max} = T_0 = \int_0^x \dfrac{q_x \mathrm{d}x}{\lambda} + T_x = \int_0^X \dfrac{q_x \mathrm{d}x}{\lambda} + T_1, \\ T_x = T_0 - \int_0^x \dfrac{q_x \mathrm{d}x}{\lambda}, \end{cases} \tag{4}$$

where T_1 is the temperature at position 1.

2.1.2 1-2 segment

The heat transfer of segment 1-2 is mainly in the vertical y-direction. According to the principle of energy conservation, the average heat flux q_H in the y-direction of the 1-2 segment is determined as follows:

$$q_H = \frac{2\int_0^{W/2} q(x)\mathrm{d}x}{H_1}. \tag{5}$$

There is an assumption for Eq. (5) that heat flux on the plate top surface is symmetric to the plate centerline.

Similarly, according to Fourier's law:

$$T_1 = q_H \Delta H / \lambda + T_{\text{channel}}. \tag{6}$$

The average heat flux on the channel wall is

$$q_{\text{channel}} = q_H H_1 / (\pi d). \tag{7}$$

According to Newton's law of cooling [30]:

$$q_{\text{channel}} = h_{\text{f}}(T_{\text{channel}} - T_{\text{f}}) = \frac{Nuk}{d}(T_{\text{channel}} - T_{\text{f}}), \tag{8}$$

where the Nusselt number Nu is determined by the empirical formula for convective heat transfer, such as the Dittus-Boelter formula for most conventional coolants. k is the thermal conductivity of the coolant. d is the hydrodynamic diameter of the cooling channel and T_{f} is the coolant temperature.

Therefore, the inner wall temperature of the cooling channel is

$$T_{\text{channel}} = \frac{q_{\text{channel}} d}{Nuk} + T_f. \tag{9}$$

Combining Eqs. (4), (6), and (9), the maximum temperature and temperature distribution function of the plate structure with active cooling are

$$\begin{cases} T_{\max} = T_0 = \int_0^X \dfrac{q_x \mathrm{d}x}{\lambda} + \dfrac{q_H \Delta H}{\lambda} + \dfrac{q_{\text{channel}} d}{Nuk} + T_{\text{f}}, \\ T_x = T_0 - \int_0^x \dfrac{q_x \mathrm{d}x}{\lambda}. \end{cases} \tag{10}$$

It is worth noting that λ is the thermal conductivity of solid material, which is a function of temperature for most materials. When Eq. (10) is used, the thermal conductivity λ is determined by an iterative calculation process.

2.2 Thermal boundary conditions

2.2.1 The model with heat flux boundary (MHF)

When the thermal boundary of the plate top surface is heat flux, for most heat flux distribution, $q(x)$ may be expressed by a polynomial such as a second-order function of the spanwise direction $q(x) = ax^2 + bx + c$, $0 \le x \le W/2$. In this paper, the second-order function is used as an example to calculate the maximum temperature and temperature distribution. According to Eq. (10), the maximum temperature and temperature distribution at the heat flux boundary condition are as follows:

$$\begin{cases} T_{\max} = T_0 = \dfrac{aX^4 + 2bX^3 + 6cX^2}{12\delta\lambda} + \dfrac{q_H \Delta H}{\lambda} + \dfrac{q_{\text{channel}} d}{Nuk} + T_{\text{f}}, \\ q_H = \dfrac{1}{3H_1}\left[2a\left(\dfrac{W}{2}\right)^3 + 3b\left(\dfrac{W}{2}\right)^2 + 6c\left(\dfrac{W}{2}\right)\right], \\ T_x = T_0 - \dfrac{ax^4 + 2bx^3 + 6cx^2}{12\delta\lambda}. \end{cases} \tag{11}$$

2.2.2 The model with convective heat transfer boundary (MCHT)

When the thermal boundary is convective heat transfer, $q(x)$ is calculated according to the following formula:

$$q(x) = h(T_{\text{hot}} - T_{\text{wall}}), \tag{12}$$

where h is the convective heat transfer coefficient, T_{wall} is the surface temperature, and T_{hot} is the hot gas temperature. The surface temperature and the heat flux are coupled to each other. The surface temperature determines the heat flux, which in turn affects the surface temperature. The heat flux distribution $q(x)$ of the MCHT model is unknown. Therefore, the maximum temperature cannot be solved directly using Eq. (10).

In many engineering cases, the convective heat transfer coefficient and hot gas temperature are nearly constants along the plate spanwise direction, and the surface temperature of the plate with active cooling is low near the plate centerline and high on both sides. Therefore, the heat flux is high near the center and low on the two sides, as shown in Fig. 2. When the convective heat transfer coefficient and the hot gas temperature are both constant, polynomial fitting is used to replace the real non-uniform heat flux distribution. In this paper, a quadratic function $q(x) = ax^2 + bx + c$, is used to approximately fit the realistic heat flux distribution. The maximum temperature and the heat flux distribution of the plate are then solved by an iterative solution method described in the next section. After obtaining the heat flux distribution, the surface temperature distribution is calculated by Eq. (11).

3. Solution method

3.1 Iterative process of the solution method

The maximum temperature of MHF model is solved directly by Eq. (11). The MCHT solution is an iterative calculation based on the assumption that the heat flux of MCHT model is nearly a quadratic function distribution. The solution flow chart is shown in Fig. 3. The solution steps are described as follows.

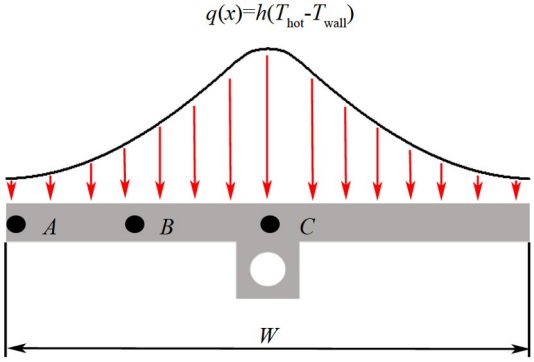

Figure 2 Schematic diagram of cooling plate of MCHT.

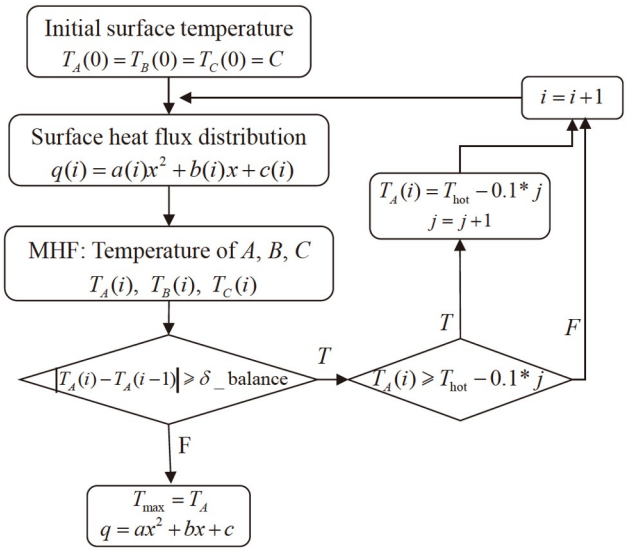

Figure 3 Solution flow chart of MCHT model.

(1) Given a uniform initial temperature, such as $T_A(0) = T_B(0) = T_C(0) = 273.15$ K. Points A and C are located on the edge and middle positions of the plate structure, respectively. Point B is located at the midpoint of A and C, as shown in Fig. 2.

(2) According to Eqs. (13)-(15), the heat flux distribution $q = ax^2 + bx + c$ is obtained.

(3) The MHF model is used to solve the temperature at points A, B, and C, as shown in Eq. (16) or (17).

(4) If $|T_A(i) - T_A(i-1)| \geq \delta\_\text{balance}$, the solution has not yet converged. δ_balance is a threshold value of the iterations, which depends on the acceptable tolerance of the error and the conductivity of the material. It is set as 1 K in this paper. i is the iteration step. For special conditions, if $T_A(i) \geq T_{\text{hot}} - 0.1j$, then let $T_A(i) = T_{\text{hot}} - 0.1j$, where j denotes the number of T_A adjustments as shown in Fig. 3. This judgment is to avoid negative heat flux on the plate surface, which would cause divergence of the solution procedure.

(5) Return to step 2 and iterate until the temperature converges.

The temperature coordinates of A, B, and C are $A(0, T_A)$, $B(W/4, T_B)$, and $C(W/2, T_C)$, respectively, and the heat flux coordinates are $A(0, q_A)$, $B(W/4, q_B)$, and $C(W/2, q_C)$, respectively. The location of the three points is shown in Fig. 2. The initial plate temperature is $T_A(0) = T_B(0) = T_C(0) = 273.15$ K. The heat flux at points A, B, and C are

$$\begin{cases} q_A = h(T_{\text{hot}} - T_A), \\ q_B = h(T_{\text{hot}} - T_B), \\ q_C = h(T_{\text{hot}} - T_C). \end{cases} \tag{13}$$

The quadratic function $q = ax^2 + bx + c$ is used to fit the real heat flux distribution. Therefore, the heat flux at points A, B, and C meet the following conditions:

$$\begin{cases} q_A = c, \\ q_B = a(W/4)^2 + b(W/4) + c, \\ q_C = a(W/2)^2 + b(W/2) + c. \end{cases} \tag{14}$$

The coefficients of the quadratic function, namely a, b, and c, are

$$\begin{cases} a = 8(q_A + q_C - 2q_B)/W^2, \\ b = (8q_B - 2q_C - 6q_A)/W, \\ c = q_A. \end{cases} \tag{15}$$

Based on Eq. (11), the temperature values of A, B, and C are calculated as follows:

$$\begin{cases} T_A = \dfrac{aX^4 + 2bX^3 + 6cX^2}{12\delta\lambda} + \dfrac{q_H \Delta H}{\lambda} + \dfrac{q_{\text{channel}} d}{Nuk} + T_{\text{f}}, \\ T_B = T_A - \dfrac{a(W/4)^4 + 2b(W/4)^3 + 6c(W/4)^2}{12\delta\lambda}, \\ T_C = T_A - \dfrac{a(W/2)^4 + 2b(W/2)^3 + 6c(W/2)^2}{12\delta\lambda}. \end{cases} \tag{16}$$

If $T_A(i) \geq T_{\text{hot}} - 0.1j$, the temperatures at points A, B, and C are calculated as follows. The initial value of j is 0.

$$\begin{cases} T_A = T_{\text{hot}} - 0.1j, \\ T_B = T_A - \dfrac{a(W/4)^4 + 2b(W/4)^3 + 6c(W/4)^2}{12\delta\lambda}, \\ T_C = T_A - \dfrac{a(W/2)^4 + 2b(W/2)^3 + 6c(W/2)^2}{12\delta\lambda}. \end{cases} \tag{17}$$

The purpose of Eq. (17) is to prevent the occurrence of temperature oscillation around T_{hot} leading to negative heat flux and to accelerate the iteration procedure as well. Based on this iterative method, the maximum temperature and heat flux distribution of the MCHT model may be obtained.

3.2 Convergence performance of the solution method

Taking the aluminum alloy and titanium alloy structures with the channel spacing W = 0.08 m as examples, the iterative solution processes of the MCHT model are shown in Figs. 4 and 5, respectively. The thermal boundary condition is h = 100 W/(m^2 K), T_{hot} = 800 K. The coolant is kerosene at 300 K, and the mass flow rate is 20 g/s. At this time, the Nu number in Eq. (9) is 56.9, which is determined by a classic heat transfer formula of the Dittus-Boelter

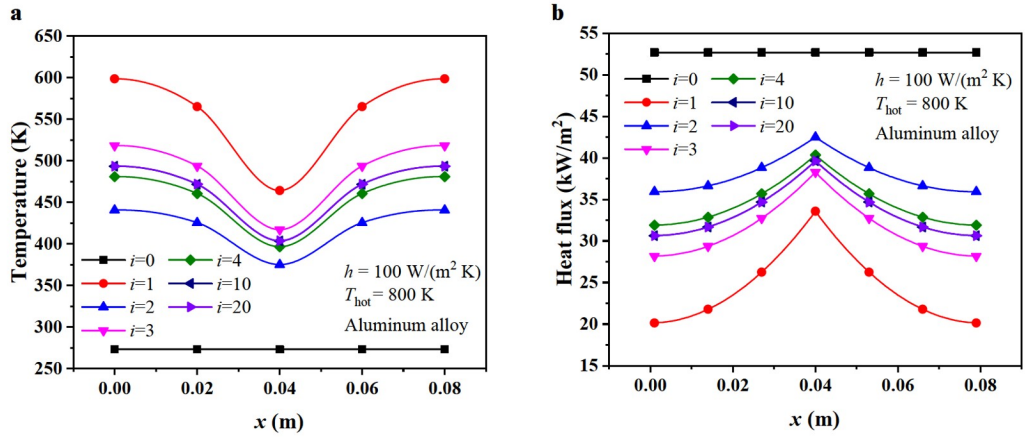

Figure 4 Solution process of MCHT model-aluminum alloy. **a** Temperature; **b** heat flux.

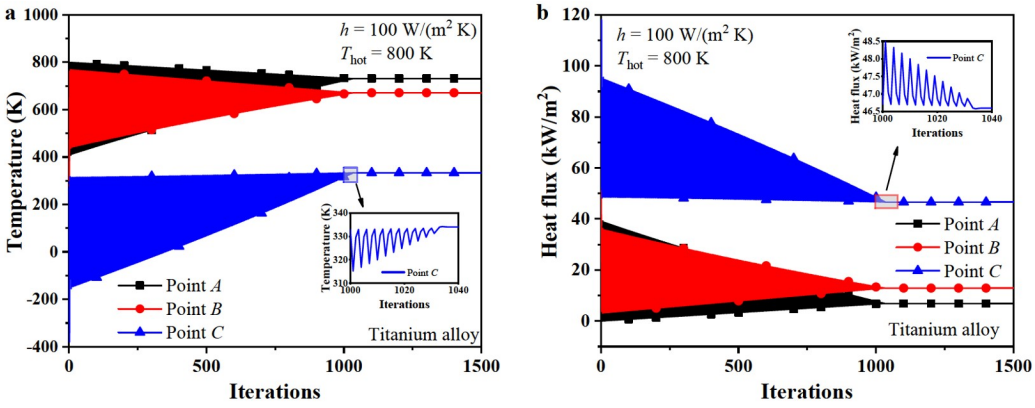

Figure 5 Solution process of MCHT model-titanium alloy. **a** Temperature; **b** heat flux.

formula described in Ref. [30].

As shown in Fig. 4, the temperature and heat flux of the aluminum alloy plate are converged after ten iterations. However, for titanium alloy plate, the convergence speed is much slower. With almost one thousand iterations, the temperature and heat flux are converged. This is because the low conductivity of titanium alloy leads to higher surface temperature, which is very close to the value of T_{hot}. Therefore, the bypass (Eq. (17)) of the iteration flow chart is launched, as shown in Fig. 3.

4. Numerical validations

The temperature distribution of plate structure with active cooling is numerically solved with the finite volume method to validate the analytical model. Navier-Stokes equation of coolant flow is solved. The RNG k-ε model [31] is used to calculate the turbulent flow of the coolant, and the near-wall region adopts the Wolfshtein turbulence model [32]. The convective terms of Navier-Stokes equations are discretized by the second-order upwind scheme, and the viscous terms are discretized by the second-order central scheme. The pressure and velocity coupling is solved by the SIMPLE method. The computational domain is divided into the solid domain and the fluid domain as shown in Fig. 6. The fluid and the solid heat transfer coupling are achieved by continuity of temperature and heat flux through the fluid/solid interface. The length of the plate (L) is 0.5 m, its width (W) varies from 0.04 to 0.1 m, and the plate thickness (δ) is 0.002 m. A 0.01 m × 0.01 m square cooling structure (H_1 × H_2) is located beneath the plate and the inner diameter of the cooling channel (d) is 0.005 m. The solid material is aluminum alloy 2a12 or titanium alloy TA15, and their material properties can be found in Ref. [33]. The fluid is RP3 kerosene and its thermophysical properties are calculated based on a 10-component surrogate model [34]. The total meshes for fluid and solid regimes in the numerical model are nearly 1.4 million. Stretched meshes are distributed in the near-wall region in the cooling channel for accurate calculation of convective heat transfer. The numerical model was validated in our previous work [35], including grid independence verification and comparison with experimental results.

The mass flow of kerosene is 20 g/s with inlet temperature and pressure of 300 K and 3.0 MPa, respectively. The thermal boundary condition on the plate top surface includes three cases: two heat flux distributions and one convective heat transfer. Taking the channel spacing of 0.1 m as an example, the two heat flux distributions are shown in Fig. 7. The thermal boundary conditions are shown in Table 1.

5. Results and discussion

In the second part of this article, an analytical model with two types of thermal conditions is established, namely MHF and MCHT. According to the numerical simulation described in the last section, the model is verified and the results are discussed in this part.

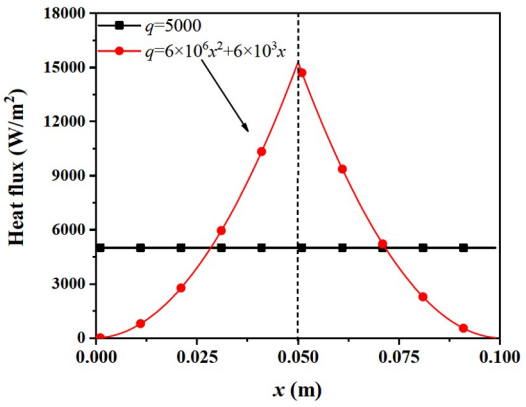

Figure 7 Heat flux distribution of W = 0.1 m.

Table 1 Thermal boundary conditions

Heat flux (W/m^2)	Values
$q_1 = ax^2 + bx + c$	$a = b = 0$, $c = 5000$
$q_2 = ax^2 + bx + c$	$a = 6 \times 10^6$, $b = 6 \times 10^3$, $c = 0$
$q_3 = h(T_{hot} - T_{wall})$	h = 100 W/(m^2 K), T_{hot} = 800 K

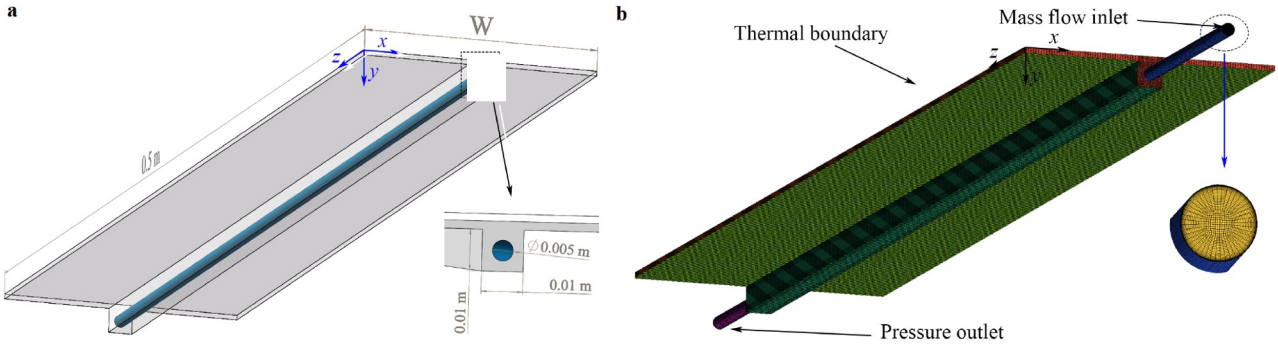

Figure 6 Computational domain. **a** Geometric configuration; **b** mesh distribution.

5.1 Verification of the MHF model

The boundary condition of the MHF model is heat flux. The heat flux distribution functions are $q(x) = 5000$ and $q(x) = 6 \times 10^6 x^2 + 6 \times 10^3 x$, $0 \le x \le W/2$, as shown in Fig. 7. The maximum temperatures of the aluminum alloy and titanium alloy plates are shown in Figs. 8 and 9 for the two heat flux conditions respectively. It can be seen from the figures that the maximum temperatures predicted by the MHF model agree well with the numerical results for varied cooling channel spacing W and materials. The maximum temperature errors are 1.8 K and 2.2 K for aluminum and titanium alloy plates respectively, accounting for 3.1% and 0.6% of the numerical temperature.

The temperature distribution is calculated by Eq. (11). Figure 10 shows the temperature distribution of aluminum

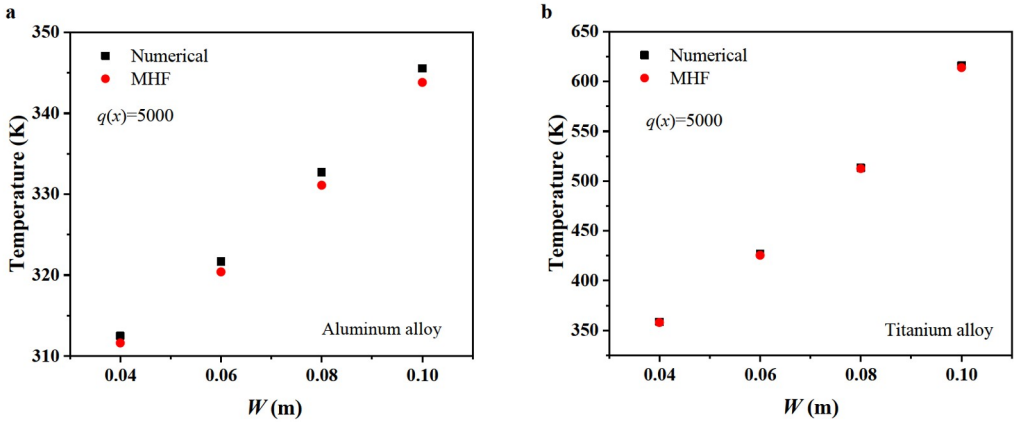

Figure 8 Maximum temperature comparisons under q_1. **a** Aluminum alloy; **b** titanium alloy.

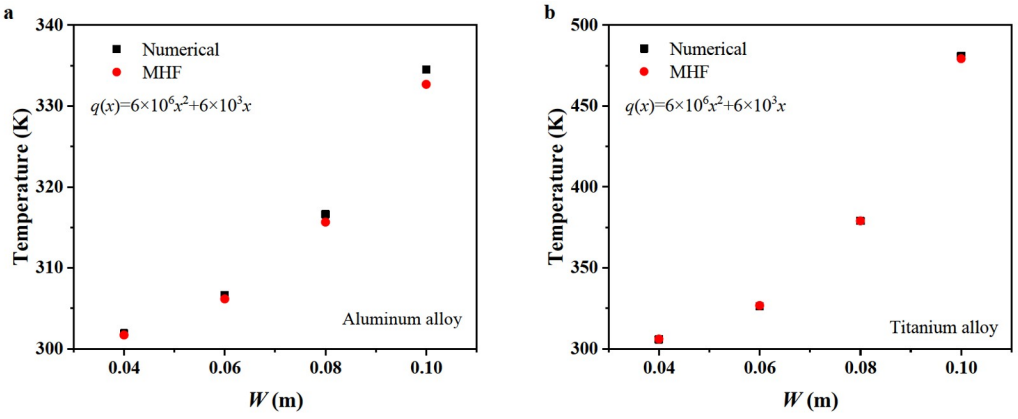

Figure 9 Maximum temperature comparisons under q_2. **a** Aluminum alloy; **b** titanium alloy.

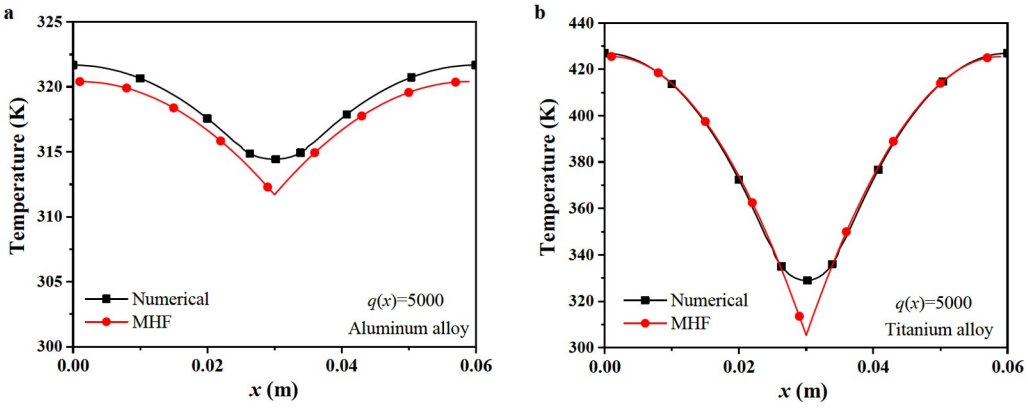

Figure 10 Temperature distribution comparisons under q_1. **a** Aluminum alloy; **b** titanium alloy.

alloy and titanium alloy when the thermal boundary is q_1 and the channel spacing W is 0.06 m. At this time, the root mean squared error (RMSE) of aluminum alloy and titanium alloy are 1.2 K and 4.7 K, respectively, accounting for 2.6% and 4.1% of the average temperature. When the thermal boundary is q_2 and the channel spacing W is 0.06 m, the temperature distribution of aluminum alloy and titanium alloy is shown in Fig. 11. The RMSE is 0.5 K and 1.8 K respectively, accounting for 1.4% and 3.7% of the average temperature.

5.2 Verification of the MCHT model

The boundary condition of the MCHT model is convective heat transfer. The MCHT model is calculated using an iterative method as described in Fig. 3. The thermal boundary conditions are listed in Table 1. The comparison of the maximum temperature of the MCHT model and the numerical model for the aluminum alloy and titanium alloy plates are shown in Figs. 12a and Fig. 13a, respectively. It can be seen from the figures that the results of the MCHT model are very close to the numerical results. The maximum temperature errors of aluminum alloy and titanium alloy are 4.9 K and 8.7 K, respectively, accounting for 1.9% and 1.8% of the numerical temperature. When the channel spacing W is 0.06 m, as shown in Figs. 12b and 13b, the RMSE of the temperature distribution of aluminum alloy and titanium alloy are 2.9 K and 14.4 K, respectively. They account for 1.9% and 4.6% of the average temperature. Through the above analysis, it can be seen that the MCHT model can accurately predict the maximum temperature and temperature distribution.

6. Conclusions

In this paper, an analytical model based on the principle of energy conservation is developed for solving the maximum temperature and temperature distribution of plate structure with active cooling. Compared with the numerical and experimental methods, the calculation time of this model is shortened to a few seconds. This model mainly considers varied thermal boundary conditions, material properties, and geometric parameters, and it is compared with the numerical model for validation. The main conclusions are as follows:

(1) The thermal boundary conditions involve heat flux and

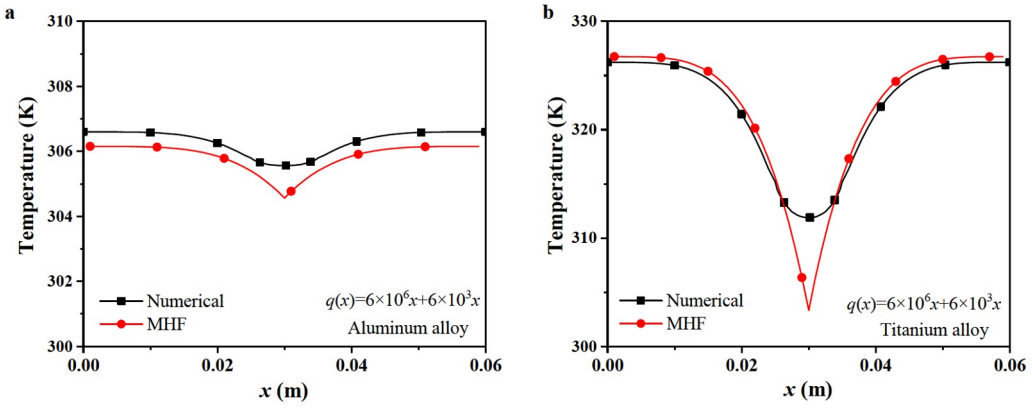

Figure 11 Temperature distribution comparisons under q_2. **a** Aluminum alloy; **b** titanium alloy.

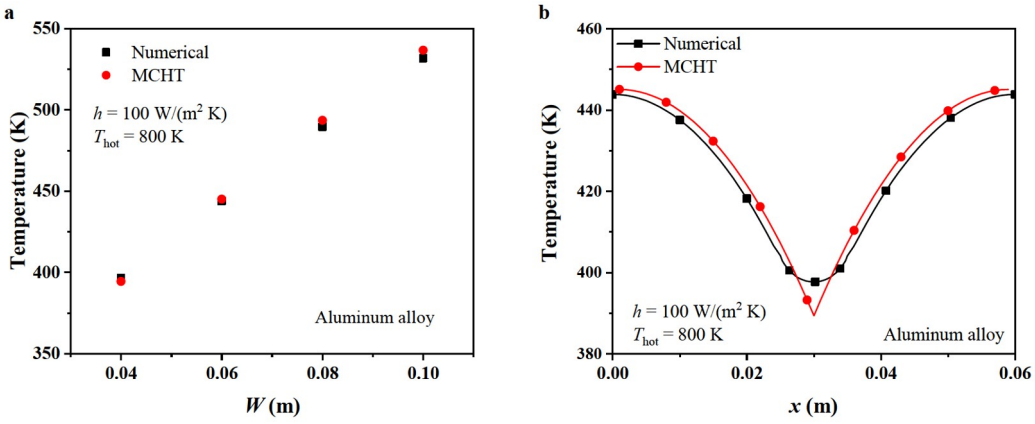

Figure 12 MCHT model results of aluminum alloy under q_3. **a** Maximum temperature; **b** temperature distribution.

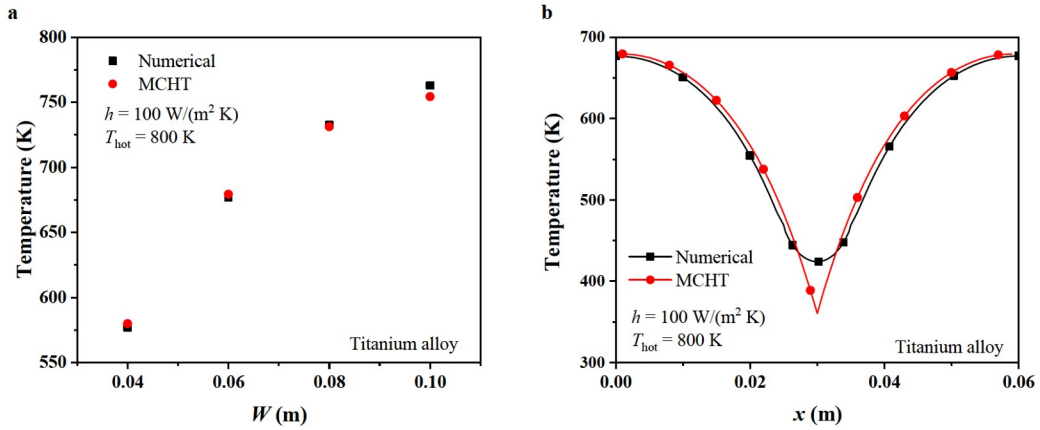

Figure 13 MCHT model results of titanium alloy under q_3. **a** Maximum temperature; **b** temperature distribution.

convective heat transfer. The MHF and MCHT models correspond to both types of boundary conditions, respectively. The MCHT model is established based on the simplification of fitting the real heat flow distribution using a second-order function.

(2) The models in this paper are able to accurately calculate the maximum temperature and temperature distribution. The maximum temperature error is within 4% compared to that of the numerical model and the RMSE of the temperature distribution is less than 5%.

(3) The models established in this paper are also suitable for a variety of materials, such as steel, copper, photovoltaic plate, water, and ethanol. It is able to quickly and accurately predict the maximum temperature and temperature distribution of plate structures with active cooling.

Author contributions *Guohao Hu, Fengquan Zhong, and Keting Chen designed the method and created the models. Guohao Hu and Fengquan Zhong wrote the first draft of the manuscript and revised and edited the final version.*

Acknowledgements *This work was supported by the National Natural Science Foundation of China (Grant No. 12072351).*

1 S. Zhang, X. Li, J. Zuo, J. Qin, K. Cheng, Y. Feng, and W. Bao, Research progress on active thermal protection for hypersonic vehicles, Prog. Aerosp. Sci. **119**, 100646 (2020).
2 J. J. Gou, Z. W. Yan, J. X. Hu, G. Gao, and C. L. Gong, The heat dissipation, transport and reuse management for hypersonic vehicles based on regenerative cooling and thermoelectric conversion, Aerosp. Sci. Tech. **108**, 106373 (2021).
3 Y. Zhu, W. Peng, R. Xu, and P. Jiang, Review on active thermal protection and its heat transfer for airbreathing hypersonic vehicles, Chin. J. Aeronaut. **31**, 1929 (2018).
4 S. Luo, D. Xu, J. Song, and J. Liu, A review of regenerative cooling technologies for scramjets, Appl. Thermal Eng. **190**, 116754 (2021).
5 X. Li, M. Du, and F. Zhong, Effect of dimple depth on turbulent flow and heat transfer of kerosene in rectangular duct, Acta Mech. Sin. **38**, 321271 (2022).
6 J. Dong, X. Zhuang, X. Xu, Z. Miao, and B. Xu, Numerical analysis of a multi-channel active cooling system for densely packed concentrating photovoltaic cells, Energy Convers. Manage. **161**, 172 (2018).
7 W. He, Y. Zhang, and J. Ji, Comparative experiment study on photovoltaic and thermal solar system under natural circulation of water, Appl. Thermal Eng. **31**, 3369 (2011).
8 H. A. Nasef, S. A. Nada, and H. Hassan, Integrative passive and active cooling system using PCM and nanofluid for thermal regulation of concentrated photovoltaic solar cells, Energy Convers. Manage. **199**, 112065 (2019).
9 S. Nižetić, E. Giama, and A. M. Papadopoulos, Comprehensive analysis and general economic-environmental evaluation of cooling techniques for photovoltaic panels, Part II: Active cooling techniques, Energy Convers. Manage. **155**, 301 (2018).
10 G. Zhao, X. Wang, M. Negnevitsky, and H. Zhang, A review of air-cooling battery thermal management systems for electric and hybrid electric vehicles, J. Power Sources **501**, 230001 (2021).
11 V. G. Choudhari, D. A. S. Dhoble, and T. M. Sathe, A review on effect of heat generation and various thermal management systems for lithium ion battery used for electric vehicle, J. Energy Storage **32**, 101729 (2020).
12 X. Zhang, Z. Li, L. Luo, Y. Fan, and Z. Du, A review on thermal management of lithium-ion batteries for electric vehicles, Energy **238**, 121652 (2022).
13 Q. L. Yue, C. X. He, M. C. Wu, and T. S. Zhao, Advances in thermal management systems for next-generation power batteries, Int. J. Heat Mass Transf. **181**, 121853 (2021).
14 L. Taddeo, N. Gascoin, K. Chetehouna, A. Ingenito, F. Stella, M. Bouchez, and B. Le Naour, Experimental study of pyrolysis-combustion coupling in a regeneratively cooled combustor: System dynamics analysis, Aerosp. Sci. Tech. **67**, 473 (2017).
15 L. Taddeo, N. Gascoin, K. Chetehouna, A. Ingenito, F. Stella, M. Bouchez, and B. Le Naour, Experimental study of pyrolysis-combustion coupling in a regeneratively cooled combustor: Heat transfer and coke formation, Fuel **239**, 1091 (2019).
16 M. S. Y. Ebaid, A. M. Ghrair, and M. Al-Busoul, Experimental investigation of cooling photovoltaic (PV) panels using (TiO_2) nanofluid in water-polyethylene glycol mixture and (Al_2O_3) nanofluid in water-cetyltrimethylammonium bromide mixture, Energy Convers. Manage. **155**, 324 (2018).
17 M. Akbarzadeh, J. Jaguemont, T. Kalogiannis, D. Karimi, J. He, L. Jin, P. Xie, J. Van Mierlo, and M. Berecibar, A novel liquid cooling plate concept for thermal management of lithium-ion batteries in electric vehicles, Energy Convers. Manage. **231**, 113862 (2021).
18 Z. Huang, Y. B. Xiong, Y. Q. Liu, P. X. Jiang, and Y. H. Zhu, Experimental investigation of full-coverage effusion cooling through perforated flat plates, Appl. Thermal Eng. **76**, 76 (2015).
19 G. Cai, C. Li, and H. Tian, Numerical and experimental analysis of heat transfer in injector plate of hydrogen peroxide hybrid rocket motor, Acta Astronaut. **128**, 286 (2016).
20 P. Pu, and Y. Jiang, Analyzing the impact of nitrogen ejection on suppression of rocket base heating, Aerosp. Sci. Tech. **107**, 106275 (2020).

21 J. Wang, Y. Li, X. Liu, C. Shen, H. Zhang, and K. Xiong, Recent active thermal management technologies for the development of energy-optimized aerospace vehicles in China, Chin. J. Aeronaut. **34**, 1 (2021).
22 W. H. Fan, F. Q. Zhong, S. G. Ma, and X. Y. Zhang, Numerical study of convective heat transfer of a supersonic combustor with varied inlet flow conditions, Acta Mech. Sin. **35**, 943 (2019).
23 Y. Wan, N. Wang, L. Zhang, and Y. Gui, Applications of multi-dimensional schemes on unstructured grids for high-accuracy heat flux prediction, Acta Mech. Sin. **36**, 57 (2020).
24 C. K. Yuan, K. Zhou, Y. F. Liu, Z. M. Hu, and Z. L. Jiang, Spectral measurements of hypervelocity flow in an expansion tunnel, Acta Mech. Sin. **35**, 24 (2019).
25 G. Tu, J. Chen, X. Yuan, Q. Yang, M. Duan, Q. Yang, Y. Duan, X. Chen, B. Wan, and X. Xiang, Progress in flight tests of hypersonic boundary layer transition, Acta Mech. Sin. **37**, 1589 (2021).
26 B. Youn, and A. F. Mills, Cooling panel optimization for the active cooling system of a hypersonic aircraft, J. Thermophys. Heat Transf. **9**, 136 (1995).
27 W. R. Wagner, and J. M. Shoji, Advanced regenerative cooling techniques for future space transportation systems, Astronaut. Aeronaut. **14**, B18 (1976).
28 Y. Z. Li, and K. M. Lee, Thermohydraulic dynamics and fuzzy coordination control of a microchannel cooling network for space electronics, IEEE Trans. Ind. Electron. **58**, 700 (2011).
29 V. S. Arpacz, Conduction Heat Transfer (Addison-Wesley Publishing Co., Massachusetts, 1966).
30 S. M. Yang, and W. Q. Tao, Heat Transfer (Higher Education Press, Beijing, 2006).
31 V. Yakhot, and S. A. Orszag, Renormalization group and local order in strong turbulence, Nucl. Phys. B-Proc. Suppl. **2**, 417 (1987).
32 M. Wolfshtein, The velocity and temperature distribution in one-dimensional flow with turbulence augmentation and pressure gradient, Int. J. Heat Mass Tran. **12**, 301 (1969).
33 M. G. Yan, B. C. Liu, and J. G. Li, China Aeronautical Materials Handbook (Standards Press of China, Beijing, 2001).
34 F. Zhong, X. Fan, G. Yu, J. Li, and C. J. Sung, Heat transfer of aviation kerosene at supercritical conditions, J. Thermophys. Heat Transf. **23**, 543 (2009).
35 G. Hu, F. Zhong, M. Du, Q. Wang, and H. Kang, Coupled heat transfer properties of aluminum/titanium alloy plates with kerosene active cooling, J. Thermal Sci. Eng. Appl. **14**, 091016 (2022).

主动冷却平板型结构件的最高温度及温度分布解析模型

胡国豪, 仲峰泉, 陈科挺

摘要 主动冷却平板型结构件应用广泛, 快速评估其温度性能具有重要意义. 本文提出了一种用于预测主动冷却平板型结构件的最高温度和温度分布的解析模型. 解析模型有三种输入参数, 包括热边界条件、材料特性和几何参数. 分别讨论了两种热边界条件下的求解过程, 包括热流密度边界和对流传热边界. 根据能量守恒原理, 建立了热流密度边界模型(MHF). 采用二次函数拟合真实热流密度分布的方法, 建立了对流传热边界模型(MCHT). 结构件的材料有铝合金和钛合金. 结果表明, 与数值模型结果相比, 该解析模型能够预测最高温度, 误差小于4%. 该模型能够快速、准确地评估主动冷却平板型结构件的热防护性能.